Improving variance estimation for time-dependent detectors in Monte Carlo dynamic calculations using adaptive sampling of neutrons

Kévin Fröhlicher, Mariya Brovchenko, Julien Taforeau, Eric Dumonteil

M&C 2023 - The International Conference on Mathematics and Computational Methods Applied to Nuclear Science and Engineering · Niagara Falls, Ontario, Canada · August 13 – 17, 2023

Improving variance estimation for time-dependent detectors in Monte Carlo dynamic calculations using adaptive sampling of neutrons

K. Fröhlicher[1]*, M. Brovchenko[1], J. Taforeau[1] and E. Dumonteil[2]

[1]Institut de radioprotection et de sûreté nucléaire, PSN-RES/SNC/LN, F-92260, Fontenay-aux-Roses, France

[2]IRFU, CEA, Université Paris-Saclay
91191, Gif-sur-Yvette, France

kevin.frohlicher@irsn.fr, mariya.brovchenko@irsn.fr,
julien.taforeau@irsn.fr, eric.dumonteil@cea.fr

ABSTRACT

Monte Carlo methods have been used for nuclear applications since the beginning of scientific computing. Decades of method refinements now allow to perform simulations of steady-state fissile systems with quite accurate results and relatively accessible computation time. Time-dependent calculations such as reactivity insertion accident simulations on the other hand still present issues. Indeed, reaching a sufficient accuracy implies high computational costs which prohibit industrial use of time-dependent Monte Carlo simulations. Dynamic calculations which include thermal feedback effects using coupled calculation schemes might especially suffer from high statistical fluctuations due to the non-linearity of multiphysics solvers. To address this issue, with the aim of reducing variance in Monte Carlo transient neutronics simulations, this article proposes a strategy based on adaptive sampling of neutron histories. The method which is proposed here is adapted from the Adaptive Multilevel Splitting method for particle transport and can make use of an importance map provided by the user. A first test of the method was conducted on a 2-dimensional 3x3 UOX assembly cluster to produce detailed and spatially integrated power distributions over time. Increases of the figure of merit up to a factor 30 were observed for detailed and spatially integrated results at the end of the neutronics transient. Such improvements of the figure of merit could eventually prove to be efficient to reduce potential amplifications of statistical fluctuations due to non-linearity of other multiphysics solvers with affordable calculation costs.

KEYWORDS: Monte Carlo, transients, Adaptive Multilevel Splitting, variance reduction

1. INTRODUCTION

Whether in the case of criticality calculations or static reactor physics, Monte Carlo methods are considered as the reference in terms of accuracy. However, a good statistical uncertainty on the result comes at the price of, sometimes, prohibitive calculation cost. Transient calculations based on Monte Carlo lead to even more difficulties as these simulations add the temporal dimension to pre-existing fission source convergence issues. Thus, despite the use of ad hoc variance reduction techniques, transient calculations still present challenges to achieve fine accuracy with affordable calculation costs [1].

The adjoint flux, taken as the neutron importance [2], has been used for variance reduction purposes for decades in static calculations [3]. While hybrid approaches based on the computation of the adjoint flux using deterministic solvers have been developed for static problems, such as CADIS [4], it is only recently that the use of such methods for dynamics simulations has gained interest [5,6], following the development of kinetics calculations in codes such as SERPENT2 [7] or TRIPOLI [8].

*Corresponding author

The purpose of this paper is to present an alternative strategy to more classical population control to reduce the variance of space- and time-dependent tallies through adaptive sampling of neutron histories. This strategy is based on the Adaptive Multilevel Splitting (AMS) method [9,10], which was implemented for particle transport [11]. The AMS has been recently extended to criticality calculations to mitigate pathological consequences of strong spatial and generational correlations [12,13]. This article presents preliminary results obtained with a proposed implementation of the AMS method in SERPENT2 kinetics mode [7,14].

2. ADAPTIVE MULTILEVEL SPLITTING METHOD

The Adaptive Multilevel Splitting method for particle transport consists in iteratively ranking and resampling neutrons histories to push particles towards a detector. It comes from applied mathematics [9,10] and was later adapted to particle transport in the context of neutron fixed source calculations [11]. More recently, its use was used in the context of reactor physics as an alternative to the power iteration based algorithm usually used in criticality calculations [13].

2.1. Detector

Since the AMS aims at improving the variance estimate by bringing more particle histories into a detector, it is important to clearly defined what is meant by *detector*.

Considering an integral quantity, such as a reaction rate, one wants to estimate by means of a Monte Carlo simulation, the general form of this score may be written as

$$X = \int_{\mathcal{D}(\vec{r})} d^3r \int_{\mathcal{D}(\vec{\Omega})} d^2\Omega \int_{\mathcal{D}(E)} dE \int_{\mathcal{D}(t)} dt f(\vec{r}, \vec{\Omega}, E, t)\phi(\vec{r}, \vec{\Omega}, E, t) \tag{1}$$

where

- $\vec{r}$, $\vec{\Omega}$, E and t are the position, direction, energy and time,
- $f(\vec{r}, \vec{\Omega}, E, t)$ is the response function that characterizes the physical quantity that is sought,
- $\mathcal{D}_{(\vec{r})}$, $\mathcal{D}_{(\vec{\Omega})}$, $\mathcal{D}_{(E)}$ and $\mathcal{D}_{(t)}$ are the subdomains of the phase-space over which one wants to know the the physical quantity, for position, direction, energy and time respectively,
- $\phi(\vec{r}, \vec{\Omega}, E, t)$ is the neutron flux.

The concept of *detector* as used in this article relates to the combination of the subdomains $\mathcal{D}_{(\vec{r})}$, $\mathcal{D}_{(\vec{\Omega})}$, $\mathcal{D}_{(E)}$ and $\mathcal{D}_{(t)}$, which represent the span of the detector over the phase-space, and the response function $f(\vec{r}, \vec{\Omega}, E, t)$ which characterizes the detector response regarding to the neutron flux.

2.2. The Adaptive Multilevel Splitting

Let us consider a set of N branching neutron histories described as discrete Markov chains in which each event of the sequence represents a neutron-nucleus collision during the neutrons random walks.

Let us also consider a detector (as defined in Section 2.1) defined over the subdomain $D = \mathcal{D}(\vec{r}) \cup \mathcal{D}_{(\vec{\Omega})} \cup \mathcal{D}_{(E)} \cup \mathcal{D}_{(t)}$. Contributing to the score in that detector is considered a rare event if the probability to find one of the histories spanning through D during an analog simulation is very low.

In that context, the AMS can be used to increase the number of histories reaching D by iteratively simulating extra Markov chains closer and closer to D. These new Markov chains are initialized by duplicating already existing histories once all random walks have been performed until the disappearance of the last particle of the history.

To select which histories will be duplicated, each history is given an importance level equal to the maximum importance reached by one of its points (i.e., the events of the Markov chain). This importance is computed

from a user-defined function, and should reflect the probability for a particle to contribute to the detection process.

Once all histories are ranked within an AMS iteration, the K worst histories regarding the importance criterion are removed from the set of N histories. At this point, K new Markov chains are initialized by duplication among the $N-K$ remaining histories, and simulated until the disappearance of the last of their neutrons to replace those that were removed.

The whole procedure is illustrated by Figure 1 for the case of a non-branching transport process with $N = 3$ histories (H1, H2 and H3) and $K = 1$.

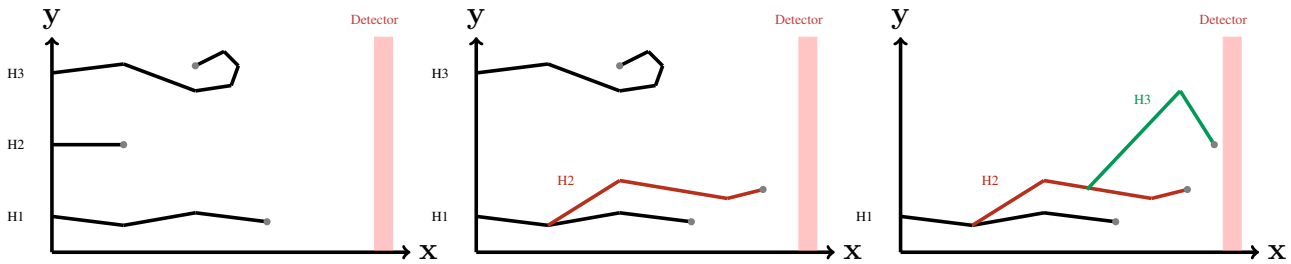

(a) Iteration 0 **(b) Iteration 1** **(c) Iteration 2**

Figure 1: AMS iterations for non branching histories (i.e., 1 history equals 1 particle) with a detector defined in the (x, y) plane, with $N = 3$ and $K = 1$. The importance function is inversely proportional to the distance to the detector.

.

Once at least $N - K + 1$ histories have reached D, the iterative algorithm stops and scores are computed by weighting the entire neutron population with

$$w_Q = \left(1 - \frac{K}{N}\right)^Q \tag{2}$$

where Q is the number of AMS iteration until the algorithm stops. Thus, if we consider an integral score one seeks to estimate using a Monte Carlo estimator noted ϕ_D, it is possible to build an unbiased estimator [10], $\hat{\phi}_D$, defined as

$$\hat{\phi}_D = \frac{w_Q}{N} \sum_{j=1}^{N} \phi_D \left(X_Q^j\right), \tag{3}$$

where X_Q^j is the j-th Markov chain (or neutron history) at iteration Q and ϕ_D is a traditional Monte Carlo estimator (e.g., collision, track-length).

In the case of fixed source calculations, this algorithm can be used to overcome spatial attenuations problems in which very few particles reach the detector location (i.e., $\mathcal{D}(\vec{r})$). The idea presented here is to overcome a time attenuation in which few neutrons reach the time of detection (i.e., $\mathcal{D}(t)$)). For subcritical systems, this attenuation arises naturally as particles tend to disappear over time. In that case, the AMS acts both as a variance reduction method thanks to the importance function provided by the user, and as a population control method as it enforces the survival of neutron histories over time to reach $\mathcal{D}(t)$).

It is also possible to recast a supercritical system into a subcritical one by decreasing the particle birth rate in the system (e.g., using biased fission) and increasing the death rate (e.g., using Russian Roulette).

For more detail about the AMS mechanics and implementation in the context of particle transport, the reader can consult Refs. [15] and [16].

2.3. Use of the branchless collisions method

To limit the number of branches inside histories, and facilitate the use of the AMS in a branching system (cf. [16]), the branchless collisions method was used. It consists in enforcing the number of particles resulting from a collision to be equal to one. Put simply, the analog treatment of collisions becomes:

- a collision may lead to a fission with a probability $\frac{\nu\Sigma_f}{\nu\Sigma_f+\Sigma_s}$, or,
- a collision may lead to a scattering with a probability $\frac{\Sigma_s}{\nu\Sigma_f+\Sigma_s}$,
- After each collision, the weight of the outgoing particle is multiplied by $\frac{\nu\Sigma_f+\Sigma_s}{\Sigma_t}$,

where ν is the mean number of neutrons emitted by fission, and Σ_s, Σ_f, Σ_t are the macroscopic scattering, fission and total cross-sections.

Since the AMS was always used in combination with the branchless collisions method in this article, the name AMS_b was used to name AMS simulations.

3. ROD DROP SIMULATION

3.1. Geometry and simulation parameters

As a proof of concept, the AMS was implemented in SERPENT2 kinetics mode and applied to a subcritical transient initiated by a control rods drop in a two-dimensional 3x3 UOX assembly cluster represented on Figure 2. Regarding the AMS implementation within SERPENT2, delayed neutron precursors are not considered for computing the importance of a history or to sample initialization points for the duplicated histories yet (although their physics is still taken into account during the transport step, as in any SERPENT2 baseline calculation).

Vacuum boundary conditions are set along x-axis and y-axis. At $t = 0s$, 24 AIC control rods are instantly placed in the central assembly, bringing the total static anti-reactivity of the cluster to $\rho = -6900$ pcm.

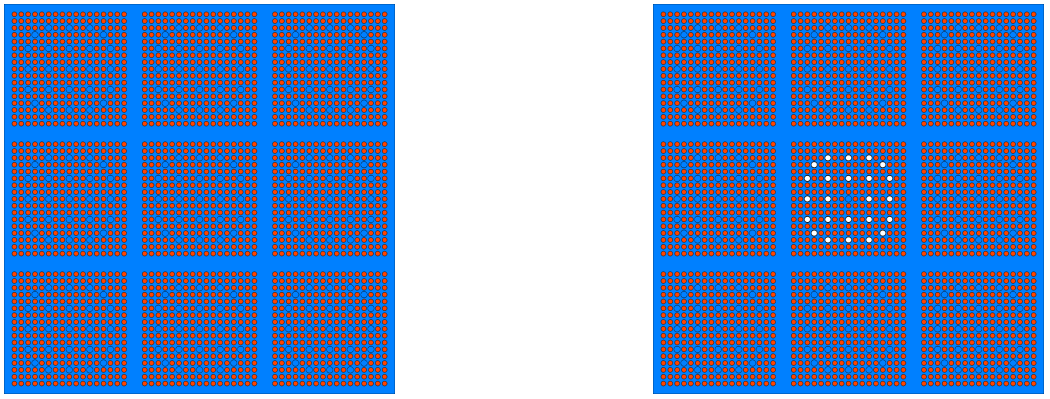

(a) Before the rod drop ($t < 0$) **(b) After the rod drop ($t \geq 0$)**

Figure 2: Cluster geometry before and after the rod drop (blue: borated water, red: fuel, white: AIC control rods, black: control rod cladding, grey: zircaloy fuel and guide tubes cladding).

To assess the AMS capabilities regarding variance reduction in a time-dependent problems, several calculations were performed using different importance functions to rank neutron histories. To compare the results to reference solutions, native SERPENT2 simulations were also performed. In total, five different sets of parameters were tested, as summarized in Table 1. Cases *AMS$_b$ central* and *AMS$_b$ outer* differ from the case *AMS$_b$* only by the importance map that is used, as detailed in the next section.

Table 1: Simulation parameters for the cluster rod drop simulation.

Case	AMS	Importance	Branchless collision	Population control
Analog	no	-	no	no
Reference	no	-	yes	every 1 ms
AMS_b	yes	t	yes	-
AMS_b central	yes	$N^*(t)\psi^*_{central}(\boldsymbol{r}, E)$	yes	-
AMS_b outer	yes	$N^*(t)\psi^*_{outer}(\boldsymbol{r}, E)$	yes	-

3.2. Importance function

As displayed in Table 1, three different importance functions were used with the AMS. First, the time of collision (t) was used as a simple way to rank histories and push particles through time in the case *AMS$_b$*. Then, two time-, energy- and space-dependent maps were considered to study the impact of the importance map on performances. These are the *AMS$_b$ central* and *AMS$_b$ outer* cases. There is no neutronics code capable of computing a real time-dependent adjoint flux to the authors knowledge, so an approximation was used. Based on the assumption of separability of time and space/energy variables, the adjoint equations of the point kinetics were used. The time-dependent part, namely $N^*(t)$, was computed using a Crank-Nicholson integration scheme in Python, while the energy- and space-depenent part ($\psi^*(\vec{r}, E)$) was generated using ADVANTG[17].

Two maps, $\psi^*_{central}(\vec{r})$ and $\psi^*_{outer}(\vec{r})$, were generated over 572x572 spatial bins and 47 energy groups:

- $\psi^*_{central}(\vec{r})$: the detector is defined as the fission rate over the central assembly (i.e., $f(\vec{r}, \vec{\Omega}, E) = \Sigma_f(\vec{r})$ and $\mathcal{D}(\vec{r}) =$ central assembly, $\mathcal{D}(\vec{\Omega}) = 4\pi$, $\mathcal{D}(E) = [0, \infty[$,
- $\psi^*_{outer}(\vec{r})$: the detector is defined as the fission rate over the 8 outer assemblies (i.e., $f(\vec{r}, \vec{\Omega}, E) = \Sigma_f(\vec{r})$ and $\mathcal{D}(\vec{r}) =$ outer assemblies, $\mathcal{D}(\vec{\Omega}) = 4\pi$, $\mathcal{D}(E) = [0, \infty[$.

The two spatial importance maps for 37.3 eV $< E <$ 101 eV are displayed in Figures 3a and 3b and correspond to cases *AMS$_b$ central* and *AMS$_b$ outer* respectively.

3.3. Numerical Results

The power was computed in 1000 times bins from $t = 0$ to $t = 10$ ms for the three AMS cases mentioned above (*AMS$_b$*, *AMS$_b$ central* and *AMS$_b$ outer*). The power was also monitored over space in each time bin over a 20x20 superimposed spatial mesh. Results were compared to the ones obtained with the *analog* baseline of SERPENT2 kinetics mode, using the Figure of Merit (FoM), here defined as

$$FoM(t) = \frac{1}{\sigma^2(t)T}, \tag{4}$$

where $\sigma^2(t)$ is the variance of the mean score at time t and T the total computation time displayed in Table 2.

By *analog* we mean here that the calculation was performed without turning on any options of the SERPENT2 kinetics mode. Meaning that no population control other than precursors forced decay [18,19], and no collision biasing technique was used. Another SERPENT2 calculation was performed using Russian Roulette and splitting as population control, and the branchless collision method to model collisions. This simulation was named *reference*, as it represents here state of the art regarding methods used in Monte Carlo kinetics calculations.

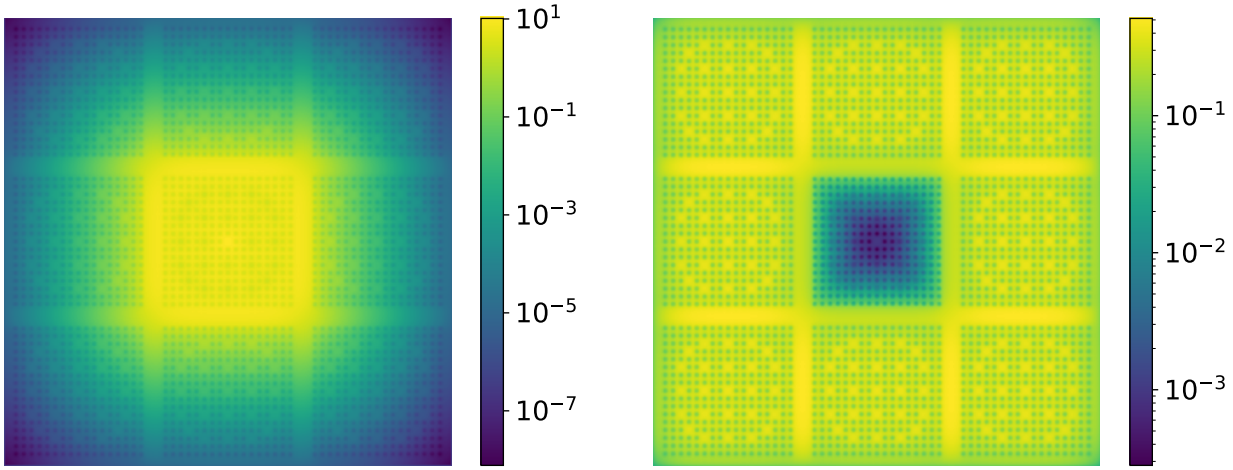

(a) $\psi^*_{central}(\vec{r})$ **(b)** $\psi^*_{outer}(\vec{r})$

Figure 3: Spatial importance distribution for the assembly cluster with AIC control rods (37.3 eV $< E < 101$ eV).

Table 2: Calculation times

Case	Total time [CPU.min]
Analog	1019
Reference	2436
AMS_b	1013

3.3.1. Spatially integrated power

The spatially integrated power results are shown in Figure 4, and regroup the power over time in the top figure, and the difference between the *AMS$_b$* simulation and the two SERPENT2 baseline calculations in terms of combined standard deviations computed as

$$\zeta(case) = \frac{P(case) - P(AMS_b)}{\sqrt{\sigma^2_{case} + \sigma^2_{AMS_b}}}. \tag{5}$$

The abscissa axis shows the transient time and is logscaled to highlight the prompt drop phase. From this figure stands out the fact that the results obtained using the AMS in kinetics are coherent with those computed with SERPENT2 version 2.1.32.

The relative standard deviations and the FoMs are displayed in Figure 5. The FoMs presented here were computed as relative FoMs compared to the *analog* case, i.e., $FoM(case)/FoM(analog)$. A prompt drop of the power occurs between $t = 0$ ms and $t = 1$ ms, during which the standard deviation increases until it stabilizes once the transient is mainly driven by delayed neutrons. Regarding SERPENT2 reference calculations (namely *analog* and *reference* cases), the *analog* case presents a higher FoM. This is due to the higher overall computation time of the *reference* case (cf. Table 2), because of population control, and the fact that population control has not started yet, hence the similar standard deviation. The branchless

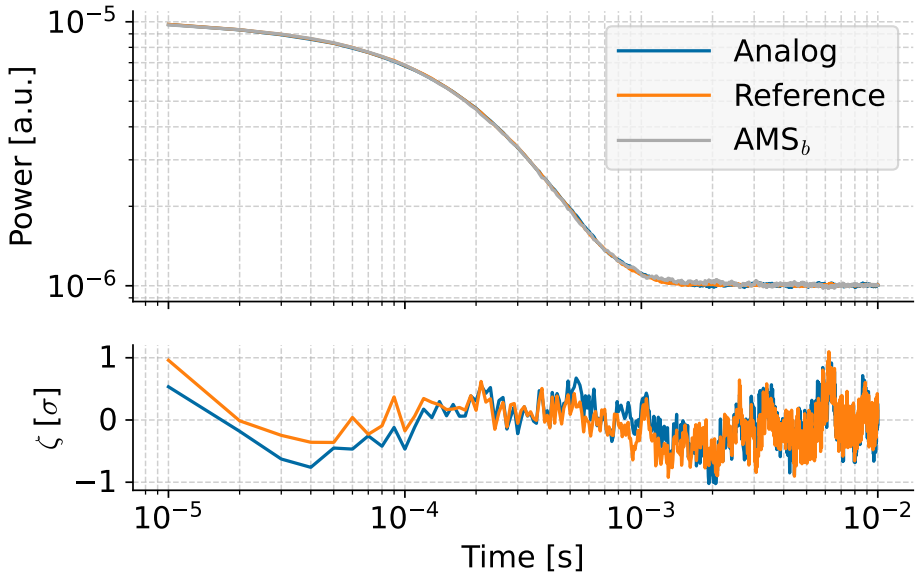

Figure 4: Spatially integrated power over time (top) and difference between the power computed with the AMS and the power computed from native SERPENT2 calculations in terms of combined standard deviation (bottom).

collisions method seems to have a low impact for subcritical systems, as previously suspected [18]. Note that the weight window parameters were left to their default value, and therefore not optimized for this specific case. The standard deviation is slightly reduced every millisecond due to the population control in the *reference* case, hence the teeth observed on the standard deviation and FoM plots.

As for AMS calculations, the error on the average results is higher (and the FoM lower) than other SERPENT2 calculations until the end of the transient, where the uncertainty drops. For the last millisecond of the transient, the FoM becomes greater than the analog FoM up to a factor 10. This result is globally positive, as the FoM was improved where the detector was defined from a temporal point of view.

3.3.2. Power spatial distribution

The distribution of the ratio $FoM(case)/FoM(analog)$ was also plotted in Figure 6 for the very last time interval. It appears that all AMS cases allowed to increase the FoM in all spatial bins at the end of the transient, since all distributions start for a FoM ratio higher than 1, in a much more efficient way than the *reference* calculation. The *AMS$_b$* simulation produced better results, with a FoM up to 40 times better than the *analog* calculation. The spatial distribution of the FoM ratio is plotted over space for the *AMS$_b$* case in Figure 7a, and shows that the improvement is rather homogeneous.

Finally, Figure 7b shows a comparison between the FoMs of the *AMS$_b$ central* and *AMS$_b$ outer* cases over space in the last time bin. No proper pattern seems to stand out as results remain noisy.

In that specific case, changing from a purely time-dependent importance map to a more complex adjoint flux does not have any effect on the spatial distribution of the FoM, except worsening the overall performances of the AMS. However, it is important to put these results into perspective in several points:

- the scope covered by a single test case is fairly insufficient to fully characterize the method,
- the implementation of the AMS within SERPENT2 may still benefit from future improvements (e.g., include delayed neutron precursors importance),

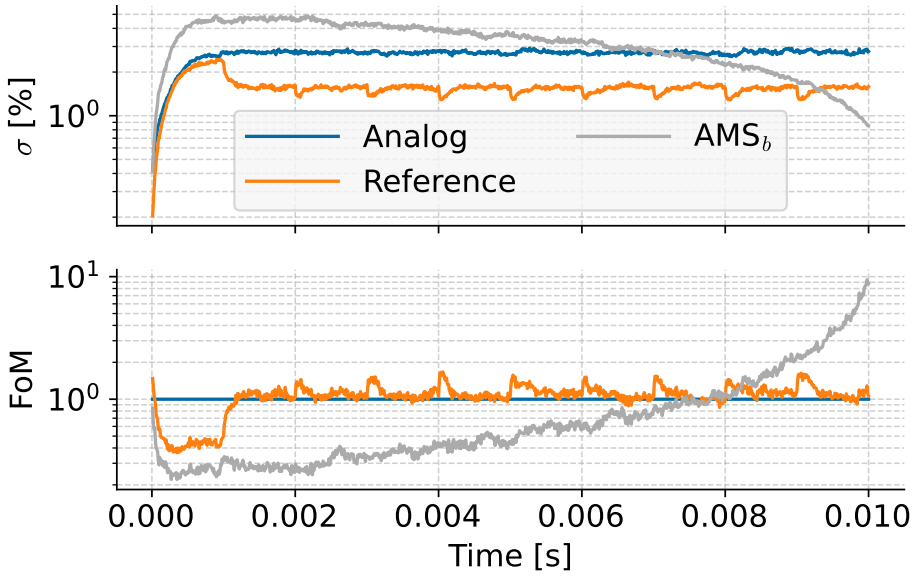

Figure 5: Relative standard error (top) and FoM (top) for the spatially integrated power. The FoM is displayed as a ratio over the FoM of the analog calculation.

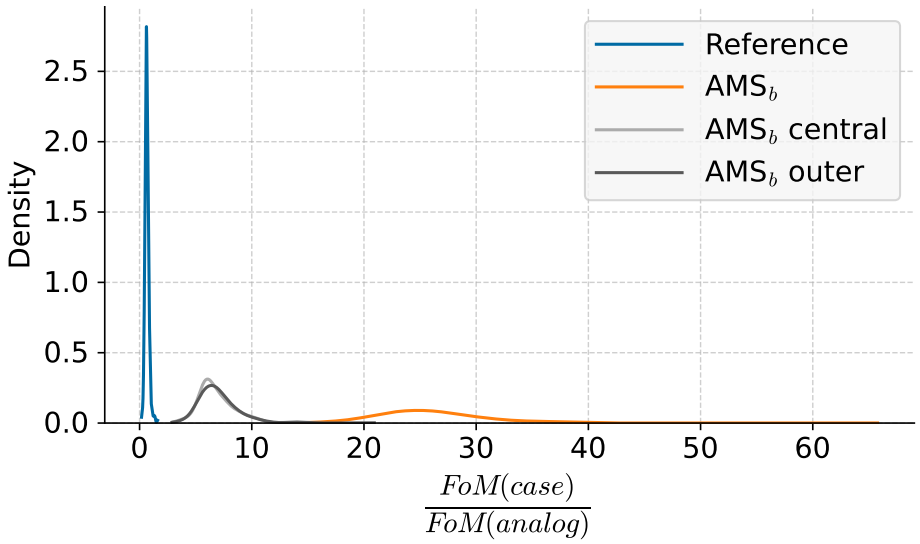

Figure 6: Relative FoM distribution for the power spatial distribution in the last time bin $\left(t \in \left[9.99 \times 10^{-3}\ \mathbf{s}, 10^{-2}\ \mathbf{s}\right]\right)$**.**

- the goal was to assess the AMS capabilities for kinetics applications, and since no true time-dependent adjoint flux are available yet, a coarse approximation was used for proof of concept purposes. Therefore, the importance function used could be very far from an ideal Green's function and thus affect the performance of the method compared to a simple importance like the one used in the *AMS$_b$* case.

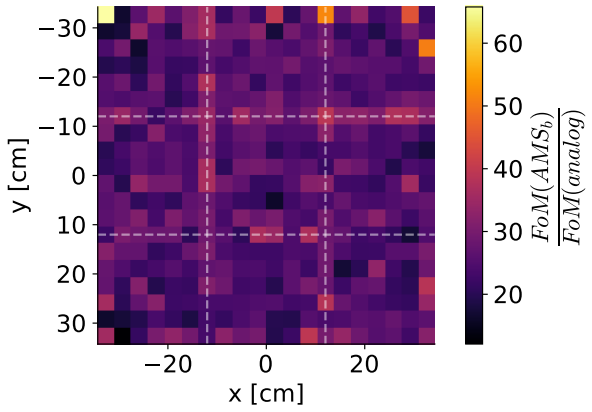

(a) AMS_b VS analog

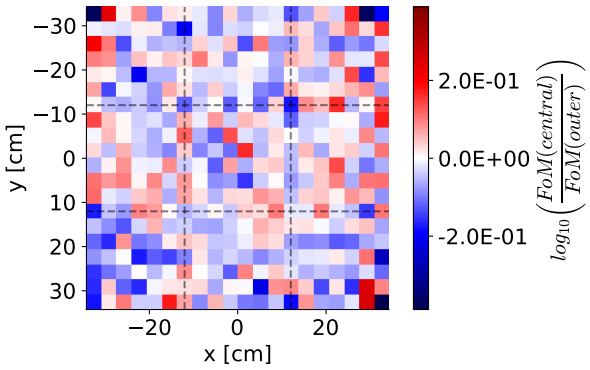

(b) AMS_b central VS AMS_b outer (log scaled: red bins mean that the case *AMS central* has a better FoM at these locations that the case *AMS outer* while blue bins mean the opposite)

Figure 7: FoM ratios for the power spatial distribution in the last time bin $\left(t \in \left[9.99 \times 10^{-3}\ \mathbf{s}, 10^{-2}\ \mathbf{s}\right]\right)$. Dashed lines mark the assemblies boundaries.

4. CONCLUSIONS

In a nutshell, the Adaptive Multilevel Splitting was implemented in the SERPENT2 Monte Carlo to perform kinetics calculations. The method was tested on a subcritical transient initiated by control rods drop over a two-dimensional 3x3 UOx assembly cluster. Preliminary results showed significant improvements can be achieved by AMS at the final time steps, considered as a "time-detector" for all AMS tests. Nevertheless, the AMS did not allow to improve the FoM over the whole simulated time interval. If the objective were to reduce the figure of merit locally in time, this could not be matter of concern. Besides, the use of a spatial-energy adjoint flux by the AMS did not provide an additional gain in this case. This might be due to several points, including the implementation of the method and the importance function that was used. Prospects regarding future improvements are considered. Overall, the method performed well compared to the ones already present in SERPENT2 kinetics mode regarding the spatial distribution of the flux at the final time of the transient. Regarding multiphysics coupling, these results could prove to be interesting to reduce the uncertainty of the power map fed to other multiphysics solvers, without degrading the calculation time.

REFERENCES

[1] D. Ferraro, V. Valtavirta, M. García, U. Imke, R. Tuominen, J. Leppänen, and V. Sanchez-Espinoza. "OECD/NRC PWR MOX/UO2 core transient benchmark pin-by-pin solutions using Serpent/SUBCHANFLOW." *Annals of Nuclear Energy*, **volume 147**, p. 107745 (2020).

[2] J. Lewins. *Importance: the adjoint function*. Pergamon Press (1965). URL https://www.osti.gov/biblio/4752764.

[3] R. R. Coveyou, V. R. Cain, and K. J. Yost. "Adjoint and Importance in Monte Carlo Application*." *http://dxdoiorg/1013182/NSE67-A18262*, **volume 27**(2), pp. 219–234 (1967). URL https://www.tandfonline.com/doi/abs/10.13182/NSE67-A18262.

[4] A. Haghighat and J. C. Wagner. "Monte Carlo variance reduction with deterministic importance functions." *Progress in Nuclear Energy*, **volume 42**(1), pp. 25–53 (2003).

[5] D. Legrady, M. Halasz, J. Kophazi, B. Molnar, and G. Tolnai. "Population-based variance reduction for dynamic Monte Carlo." *Annals of Nuclear Energy*, **volume 149**, p. 107752 (2020).

[6] D. Mancusi and A. Zoia. "Zero-variance schemes for kinetic Monte Carlo simulations." *The European Physical Journal Plus 2020 135:5*, **volume 135**(5), pp. 1–33 (2020). URL https://link.springer.com/article/10.1140/epjp/s13360-020-00387-8.

[7] J. Leppänen. "Development of a dynamic simulation mode in SERPENT 2 Monte Carlo code." In *M&C 2013*, pp. 117–127. American Nuclear Society, Sun Valley, Idaho (2013).

[8] B. L. Sjenitzer and J. E. Hoogenboom. "Implementation of the dynamic Monte Carlo method for transient analysis in the general purpose code Tripoli." In *M&C 2011: International conference on mathematics and computational methods applied to nuclear science and engineering*. Rio de Janeiro, Brazil (2011). URL http://inis.iaea.org/Search/search.aspx?orig_q=RN:48022327.

[9] F. Cérou and A. Guyader. "Adaptive Multilevel Splitting for Rare Event Analysis." *https://doiorg/101080/07362990601139628*, **volume 25**(2), pp. 417–443 (2007). URL https://www.tandfonline.com/doi/abs/10.1080/07362990601139628.

[10] C. E. Bréhier, M. Gazeau, L. Goudenège, T. Lelièvre, and M. Rousset. "Unbiasedness of some generalized adaptive multilevel splitting algorithms." *https://doiorg/101214/16-AAP1185*, **volume 26**(6), pp. 3559–3601 (2016). URL https://projecteuclid.org/journals/annals-of-applied-probability/volume-26/issue-6/Unbiasedness-of-some-generalized-adaptive-multilevel-splitting-algorithms/10.1214/16-AAP1185.fullhttps://projecteuclid.org/journals/annals-of-applied-probability/volume-26/issue-6/Unbiasedness-of-some-generalized-adaptive-multilevel-splitting-algorithms/10.1214/16-AAP1185.short.

[11] H. Louvin, E. Dumonteil, T. Lelièvre, M. Rousset, and C. M. DIop. "Adaptive Multilevel Splitting for Monte Carlo particle transport." *EPJ Web of Conferences*, **volume 153**, p. 06006 (2017). URL https://www.epj-conferences.org/articles/epjconf/abs/2017/22/epjconf_icrs2017_06006/epjconf_icrs2017_06006.html.

[12] K. Fröhlicher, E. Dumonteil, L. Thulliez, J. Taforeau, and M. Brovchenko. "Improving the variance in monte carlo criticality calculations with adaptive multilevel splitting." In *International Conference on Physics of Reactors (PHYSOR 2022)*, pp. 2512–2521. American Nuclear Society, Pittsburgh, PA (2022).

[13] K. Fröhlicher, E. Dumonteil, L. Thulliez, J. Taforeau, and M. Brovchenko. "Generational variance reduction in Monte Carlo criticality simulations as a way of mitigating unwanted correlations." *Nuclear Science and Engineering*, **volume (to be published)** (2023). URL https://arxiv.org/abs/2301.03882v1.

[14] J. Leppänen, M. Pusa, T. Viitanen, V. Valtavirta, and T. Kaltiaisenaho. "The Serpent Monte Carlo code: Status, development and applications in 2013." *Annals of Nuclear Energy*, **volume 82**, pp. 142–150 (2015).

[15] H. Louvin. *Development of an adaptive variance reduction technique for Monte Carlo particle transport*. Ph.D. thesis, Université Paris-Saclay (2017). URL https://tel.archives-ouvertes.fr/tel-01661422.

[16] K. Fröhlicher. *Improving Monte Carlo reactor physics simulations using adaptive sampling of neutron histories*. Ph.D. thesis, Université Paris Saclay (2023).

[17] S. W. Mosher, S. R. Johnson, A. M. Bevill, A. M. Ibrahim, C. R. Daily, T. M. Evans, J. C. Wagner, J. O. Johnson, and R. E. Grove. "ADVANTG An Automated Variance Reduction Parameter Generator, Rev. 1." Technical report, Oak Ridge National Laboratory (ORNL), Oak Ridge, TN (United States) (2015). URL http://www.osti.gov/servlets/purl/1210162/.

[18] B. Sjenitzer. *The dynamic Monte Carlo method for transient analysis of nuclear reactors*. Ph.D. thesis, Delft university of technology (2013). URL https://www.narcis.nl/publication/RecordID/oai:tudelft.nl:uuid:6a4bfa4c-2d1f-4648-9698-6eb7ec7e2d11.

[19] V. Valtavirta, M. Hessan, and J. Leppänen. "Delayed neutron emission model for time dependent simulations with the Serpent 2 Monte Carlo code - First results." In *PHYSOR 2016 : Unifying Theory and Experiments in the 21st Century*, pp. 1568–1582. American Nuclear Society, Sun Valley (2016).